Korean Chem. Eng. Res., 62(2), 191-199 (2024)
https://doi.org/10.9713/kcer.2024.62.2.191
PISSN 0304-128X, EISSN 2233-9558

Thermo-hydraulic Effect of Tubular Heat Exchanger Fitted with Perforated Baffle Plate with Rectangular Shutter-type Deflector

Md Atiqur Rahman†

Department of Mechanical Engineering, Birla Institute of Technology, Mesra, Ranchi, Jharkhand, 835215, India
(Received 21 October 2023; Received in revised from 5 February 2024; Accepted 8 April 2024)

Abstract – A study was conducted on a tubular heat exchanger to improve its heat transfer rate by using a novel baffle plate design with discontinuous swirling patterns. The design consisted of perforated baffle plates with rectangular air deflectors positioned at varying angles. The tubes in the heat exchanger were arranged in a consistent alignment with the airflow direction and exposed to a uniform heat flux on their surfaces. Each baffle plate included sixteen deflectors inclined at the same angle and arranged in a clockwise pattern. This arrangement induced a swirling motion of the air inside a circular duct where the heated tubes were located, leading to increased turbulence and improved heat transfer on the tube surfaces. The spacing between the baffle plates was adjusted at different pitch ratios, and the Reynolds number was controlled within a range of 16,000 to 29,000. The effects of pitch ratios and inclination angles on the heat exchanger's performance were analyzed. The results indicated that using a baffle plate with rectangular deflectors inclined at 30° and a pitch ratio of 1.2 resulted in an average increase of 1.29 in the thermal enhancement factor.

Key words: Inclination angle, Flow resistance, Circular baffle plate, Rectangular shutter type deflector, Discontinuous swirl flow, Thermo-fluid performance

1. Introduction

Augmenting HT is of extreme prominence as it leads to more efficient energy usage, allows for compact and lightweight system designs, increases the reliability and lifespan of equipment, and enables effective thermal management in electronic devices. In recent years, numerous approaches have been projected to accomplish this, branded as active and passive techniques. Passive methods, which are widely implemented due to their independence from external power sources, comprise twisted tapes, surface roughness, wire coils, baffles, ribs, VG, fins, and jet impingement. These passive methods can improve total system efficiency, decrease energy intake, and drive technological advancements in different industrial sector.

The mentioned methods are commonly referred as turbulence enhancer/promoters. They involve incorporating structures or devices in the fluid flow path to create or boost turbulence by generating secondary vortex flow along with the main flow. Turbulence promotes better mixing, leading to increased heat transfer rates by enhancing convective HT between the fluid and the solid surface. This is attained by enhancing fluid mixing, disruption of thermal boundary layers, and increased fluid velocities.

Researchers have shown growing interest in swirlers, also known as swirl-producing devices or swirl generators, which are used to create rotational flow in fluids. These devices have various applications in heat transfer, improving heat transfer rates, fluid mixing, and flow control. Swirl flow involves the fluid rotating around a central axis, either through a tangential velocity component or the presence of vortices. It plays a significant role in different engineering systems, such as pipes, pumps, cyclones, and tornadoes, affecting factors like mixing, heat transfer, and pressure drop. When it comes to heat transfer applications, swirl-producing devices are vital as they enhance convective heat transfer coefficients, resulting in more efficient heat exchange. The swirling motion increases the contact area between the fluid and heated surface consequently, improving heat transfer and redistributing heat more evenly. Additionally, these devices can stabilize flow and optimize heat transfer performance in certain systems, like heat exchangers with parallel flow passages.

Swirl flow without any reaction involved finds practical applications in various devices such as vortex amplifiers and reactors, heat exchangers, cyclone separators, whirlpools, jet pumps, tornadoes [1-6], and many more. However, when there is a reaction involved, swirlers are widely utilized in combustion systems such as industrial furnaces, gas turbines, gasoline and diesel engines, boilers, and different heating devices. The swirl flow in combustion has versatile effects on mixing, aerodynamics, combustion intensity, flame stability, and emissions of pollutants.

Heat exchangers can generate swirl flow by modifying the geometry of either the tube side or the duct side. This can be done by adding ribs, deflectors, fins, or vanes [7-10]. For example, in a STHX employed for condensation, a hot vapour flows through the tubes while a cooling fluid flows on the shell side. To enhance the

† To whom correspondence should be addressed.
E-mail: rahman.md4u@gmail.com

heat transfer process, swirl-generating devices like twisted tape inserts or helical baffles can be inserted within the tubes or shell. These devices create swirling flow, leading to improved HT rates. Some studies have investigated the impact of retrofitting on tube or duct, to generate flow maldistribution to augment h_m.

Liu and Zhang [11] numerically investigated a novel fin design to enhance the HT properties of the triple-tube latent heat storage system (TTLHSS). Initially, a comparison was conducted between the melting process with no fins and newly introduced fins. The melting and solidification duration decreased by 67.7% and 74.8%, respectively, compared to the case without fins. Subsequently, the impact of the new fin's thickness, length ratio, and angle on the PCM's melting and solidification process was investigated. The liquid fraction distribution and PCM's time-dependent liquid fraction curve under different conditions were analyzed. The findings demonstrated that including the new fins pointedly enhanced the heat storage and release rate of PCM in TTLHSS. Unlike rectangular fins, the melting and solidification durations were diminished by 32.7% and 52.9%, respectively. The optimal fin configuration, with a fin thickness of 0.8 mm, fin length of 1, and an angle of 63.1°, substantially reduced the overall time by 84.5% compared to HX without fins.

Hussein and Hameed [12] inspected the efficiency of a dual-tube HX in facilitating the heat transfer between air and water. Segmental baffles with semi-circular apertures were implemented on the outside of the heat exchanger to enhance the heat transfer process. These baffles were comprised of semi-circle shaped fins. Air was employed in the outer region, while water circulated within the inner tube. The experiments encompassed seven different air *Re*, varying between 2700-4000 while maintaining the waterside *Re* at 34,159.

Moreover, the study investigated the impact of three different semi-circular perforation sizes (30, 25, and 20 mm) on the heat exchanger's thermal efficiency. Several parameters were assessed, including the *Nu*, h_m, *f*, and thermal enhancement factor (TEF). A comparison was also made between the heat exchanger with and without baffles. The findings revealed a substantial enhancement in HT efficiency with the implementation baffles. The average h cm increased 29.7%, 62%, and 80.6% when employing baffles with 30, 25, and 20 mm perforation sizes, respectively. Furthermore, the TPF of the HX surpassed unity in all tested cases with baffles, with the utmost thermal performance achieved when using baffles with a 20 mm perforation size.

Bahuguna *et al*. [13] examined entropy generation in a heat exchanger tube incorporating vortex generator inserts with three blades. The efficiency of the HX was assessed using the entropy generation number for augmentation. The analysis was based on experimental data from tests on a tube equipped with vortex generator (with triple-blade) inserts. The inserts have varying geometric parameters, such as pitch ratio (2, 3, and 4) and perforation index (0% and 25%). The operational parameter, represented by *Re*, varied from 6,000 to 24,000. The findings revealed that at a 1% and 0% pitch ratio perforation index, the maximum *Nu* and *f* were recorded as 252.4 and 3.10, respectively. Comparatively, the entropy generation rate in the tube with vortex generator inserts was lower than that in a smooth tube. Heat transfer contributed significantly more to entropy generation than friction. All intensification entropy generation numbers were less than 1, with the lowest value achieved at a PR of 1 and 0% perforation index.

Mousavi A. *et al*. [14] analyzed hydraulic and thermal efficiency of a helical heat exchanger. The heat exchanger had a swirl generator with an outer curved blade and a semi-conical section with two inner holes. Two geometrical factors, the length of the swirl generator (L1) and its position (S), were studied. Using commercial software, it was observed that the swirl generator's shorter length had the most significant impact on thermal performance. Specifically, L1 model with a length 100 mm and m = 0.008 kg/s exhibited a performance enhancement of 17.65%, 53.85%, and 100% equated to the models with L1 = 200 mm, L1 = 300 mm, and no swirl generator. Additionally, the highest h_m and average *Nu* were observed when the swirl generator was positioned at $S = 0.3\pi$ mm, resulting in a thermal performance improvement of 11.11%, 53.84%, and 100% compared to the cases with $S = 0.1\pi$ mm, $S = 0.5\pi$ mm, and no swirl generator, respectively.

Leon Hui [15] carried out an experimental investigation on the influence of the spacing between rotating turbulator inserts in a heat exchanger operating with forced convection in a turbulent flow. Turbulator inserts led to a noteworthy increase in the *Nu*, with a 360% rise for non-rotating cases and a 240% increase for rotating cases. However, it also resulted in a noticeable rise in the friction factor due to the disturbance created by the turbulator inserts. By dipping the distance amongst turbulator inserts, both *Nu* and *f* were further enhanced. This phenomenon can be credited to the splitting effect of the turbulator inserts on the tube, which induced swirling flow, thus promoting forced convection. A second-law analysis indicated that the non-rotating configuration exhibited a 202% higher entropy generation rate than the rotating configuration. This implied that rotating turbulator inserts were more thermodynamically favourable, significantly improving thermal performance while reducing entropy generation.

The axial flow heat exchanger is a unique type of tubular heat exchanger that aims to improve heat transfer efficiency by introducing swirling airflow around a tube bundle carrying hot water. This is achieved by incorporating circular baffle plates with trapezoidal flow diverters [16,17] at different angles while maintaining the tube configuration. Each baffle plate contains four flow diverters at the same α, generating a swirling flow within an HX containing tube bundle. This swirling flow surges turbulence in the duct, ensuing in higher HT rates from the tube surface. The researchers conducted experiments with different baffle spacing and α of the diverters and found that a heat exchanger with a 50^o inclined diverter and a distance ratio of 1.4 exhibited the highest thermal and fluid performance, improving by 3.75 times when equated with other configurations.

Also, the effect of two trapezoidal deflectors [18] was compared. Another study by Rahman investigated the effects of rectangular punched holes with one [19] or two flow deflectors [20] and found that a single flow deflector increased thermal-fluidic performance by 41.49%. However, using two flow deflectors that were oppositely oriented [21] decreased thermal efficiency compared to HX with SBP. Further comparison of TEF by changing the geometry of deflectors to triangular [22] was studied. Rahman [23] also applied the idea of punched hole with deflectors to a conical baffle plate and achieved a 22% enhancement in TEF.

The provided passage discusses the advantages of incorporating devices that induce flow rotation in HX to enhance fluid mixing and heat transfer. These devices enhance interaction between fluids and heat transfer surfaces, resulting in higher coefficients of HT. Moreover, they prevent the accumulation of deposits on the surfaces by continuously stirring the fluid. Consequently, heat exchangers equipped with these devices exhibit improved thermal efficiency, low energy input, causing cost savings and improved system efficiency. Additionally, the use of swirling flow allowed the creation of more compact heat exchangers that can achieve efficient heat transfer with small HT surface area, reducing the overall size of HX. Furthermore, these devices eradicated stagnant flow regions and ensured an even temperature profile over the heat-transferring area, which was crucial in applications requiring consistent temperature profiles. Recent advancements in this field involved the development of innovative types of devices that induce rotation, such as conical rings, twisted tape, and helical coils, which augment HT while minimizing pressure drop. Nevertheless, the exploration of baffle plates as turbulence-inducing elements in HX and the practicality of using air as the HT fluid have been limited. Thus, the current work addresses this research gap by designing and experimenting with a novel type of swirl inducer using shutter-type rectangular deflectors installed on baffle plates to encourage fluid rotation and generate turbulence. The experimental testing will emphasize two key variables: the ratio of duct diameter to baffles spacing (PR) and the deflector angle (α). By changing these constraints, the study seeks to evaluate the superior performance achieved by using shutter-type baffles over ducts without baffle plates. The testing will be conducted under identical conditions, covering *Re* between 15,000 and 30,000. The results of this investigation have significant potential in the design of compact HX for improved HT of duct side fluid.

2. Materials and Methods

2-1. Experimental setup and HX details

The schematic is revealed in Figure 1 and comprised of several components, including HX, hot water delivery loop, air supply, DAC-assisted pressure, and temperature procurement system. An inverter-controlled HD 162A (axial fan) with an entry length of 3 m drawn in atmospheric air into the test section. Thermocouple probes inlet (T1) and outlet (T2) of the HX measured air temperature using calibrated 5 mm T-type copper-constantan thermocouples inserted into the air duct as per ASHRAE standard [24]. The temperature change was continuously monitored and recorded. ISO 5801 standards were utilized to evaluate air flow rate through a calibrated orifice plate. Six pressure ports were developed to evaluate the average differential Δp within the test section using a Labview program, the VDAS DAQ card and 0-1 psi differential transducers Δp and Δp_0. Hot water at 55 ℃ and 4 LPM was supplied to the HX using a feed pump and flow meter. Three baffle plates were placed

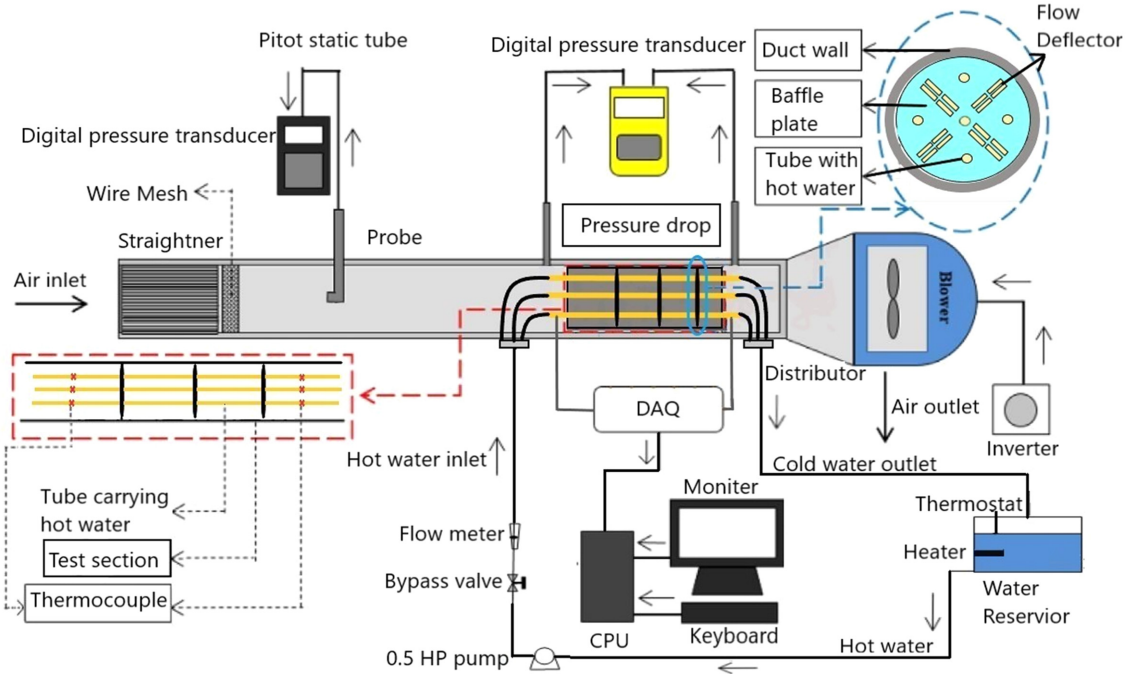

Fig. 1. Schematic of experimental setup.

equidistantly within the HX to support the tubes. Rahman [17] described the baffle plate and tube arrangement in depth.

The test section/HX was an acrylic duct with D=19 cm and a thickness of 5 mm. DHP Copper tube bundles were arranged in a circular array, with one at the center and the other at a distance of 4 cm set with its d=1 mm. Hot water traveled in these tubes whose surface temperature was acquired using ten (J-type) thermocouples (numbered t_3-t_7 at the inlet and t_8-t_{12} at the outlet), DAQ assistant NI-9213 thermocouple modules with digital readout through LabView software, and a resolution of 0.05 ℃. Before recording data, the system was allowed to stabilize. Once the system reached a stabilized state, the air temperatures at the HX inlet and outlet and the surface temperature of copper tubes were documented. The accuracies of the measuring instruments like flow meter, temperature, and pressure measurement instrument were ±0.006 kg/s, 0.5 ℃, and 0.1Pa, respectively. The accuracy of direct measurement instruments was estimated using the root mean sum square approach. The uncertainties were determined according to the Coleman and Steele method [25]. The uncertainty associated with Re was ±1.73, Nu was ±2, v was ±6, f was ±4.22 and Q was ±5.

2-2. Baffle plate details

The arrangement of the five tube configurations on the Shutter Deflector Baffle Plate (SDBP) is depicted in Figure 2(a). One tube was positioned at the center, while the others formed a circular array 4 cm away from the baffle plate's center. The innovative baffle plate consisted of sixteen rectangular openings (3×1 cm) at a distance of 15 mm from the center, through which air entered the duct. To amend the airflow from axial to swirl flow, rectangular deflectors of identical dimensions were affixed to the baffle plate at a desired angle, as shown in Figure 2(b). These configurations induced axial flow rotation, resulting in an ideal plug flow within the test section while passing over the tube bundles. Unlike the traditional deflector baffle, the baffle with deflectors did not create any dead zones in its vicinity. The swirling motion greatly enhanced mixing and heat transfer, although it led to some pressure drop. Notably, the spacing of baffle plates governed the flow's turbulence and rotation. For experimentation purposes, four-pitch ratios (PR) were chosen: 0.6, 0.8, 1, and 1.2. These rectangular deflectors were inclined at an angle (α_1-α_4) to the baffle plane, forming a circular array as depicted in Figure 2(c). Three different models were created by changing α, between 30°-50°. By inclining the deflectors, passages or flow areas were created for air to circulate. The flow area changes were based on α, the height of which was denoted by h1 and h2, as seen in Fig. 2(c). The deflectors were situated at a radial spacing of 1.5d from the center of the Baffle Plate, where d represents the outer diameter of the copper tube (10 mm).

2-3. Design restriction of study

Pitch ratio [16,17]

$$PR = {}^{l}\!/_{D}$$

Blockage ratio [18,19,20]

$$BR = {}^{S}\!/_{X}$$

$$S = X - (16 \times P)$$

In the present examination, three sets of samples of SDBP with inclination angles of (α=30, 40 and 50°) were 3D printed and installed in an HX with longitudinal flow having a constant BR of 0.70. The information acquired was then scrutinized to conclude the consequence of PR and α on the TEF of the HX.

2-4. Data Reduction

Cao's [26] method was engaged to assess $h_{c,m}$ Reynolds number (Re)

$$\mathrm{Re} = \frac{\rho \cdot v \cdot \mathrm{D}_h}{\mu} \tag{1}$$

ρ and μ of air were calculated at the mean temperature of the air (intake and outlet).

$$v = \sqrt{\frac{2\Delta P}{\rho}} \tag{2}$$

$$h_{c,m} = \frac{Q}{A_p \Delta t_{lm}} \tag{3}$$

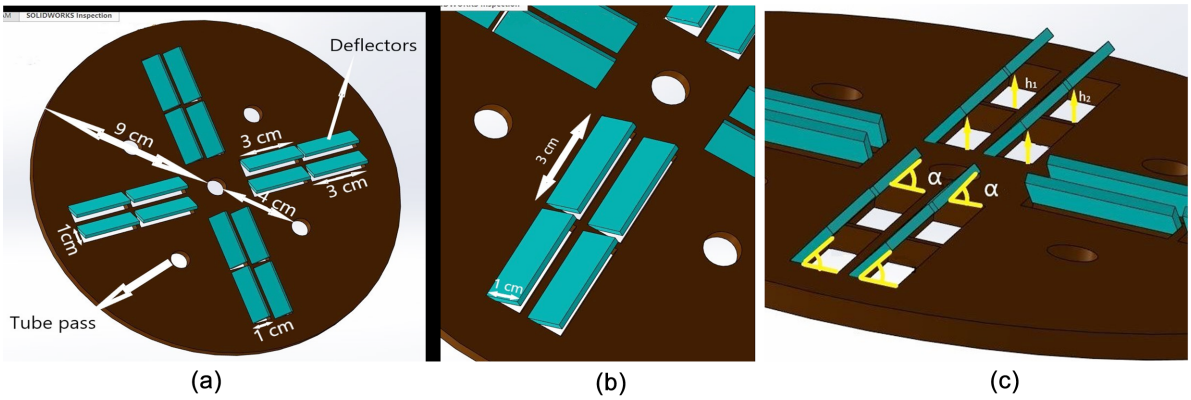

Fig. 2. (a) CAD model of SDPB (19 cm) diameter; (b) Rectangular Deflector dimension; (c) Deflector flow area and α details.

Q of air

$$Q = C_p \rho v A_c \left(T_2 - T_1\right) \tag{4}$$

T_2 and T_1 were the air temperatures leaving and entering the HX. Δt_{lm} was assumed as

$$\Delta t_{lm} = \frac{\left(T_{w,in} - T_1\right) - \left(T_{w,out} - T_2\right)}{ln\left(T_{w,in} - T_1\right) / \left(T_{w,out} - T_2\right)} \tag{5}$$

where $T_{w,in}$ and $T_{w,out}$ was the average temperature captured at the copper tube surface, calculated as

$$T_{w,in} = \left[\frac{\sum_{3}^{7} T_i A_i}{A_p}\right]_{in}, T_{w,out} = \left[\frac{\sum_{8}^{12} T_i A_i}{A_p}\right]_{out} \tag{6}$$

The typical Nu, f, and j depicted the duct's fluid flow and thermal attributes.

$$Nu = \frac{h_m D_h}{\lambda} \tag{7}$$

$$j = \frac{Nu}{RePr^{1/3}} \tag{8}$$

$$f = \frac{2\Delta p D}{\rho v^2 L} \tag{9}$$

From Eq. (3), in addition to Eq. (4)

$$h_{c,m} = \frac{C_p \rho v A_c (T_{a,out} - T_{a,in})}{A_p \Delta t_{lm}} \tag{10}$$

Variables like heat transfer augmentation (j/j_0), relative flow resistance (f/f_0), and TEF [$(j/j_0)/(f/f_0)^{1/3}$], respectively, were employed where f_0 and j_0 represented the acquired friction and Colburn factor for a duct without baffles was utilized as a reference. At the same time, f and j denoted the analogous values for a duct with SDBP [17,18,19].

2-5. Validation of experimental result

The accuracy of the experiment can be assessed by equating the obtained values of Nu and f from Equations 7 and 9 with the equations proposed by Gnielinski [27], Dittus and Boelter [28] for Nu, and Blasius [29] and Colebrook-White [30] for calculating f. This comparison helped to determine the precision of the experimental outcomes. On average, a positive deviation of 6.172 with Dittus and Boelter, a negative deviation of 8.091 for Gnielinski, a negative deviation of 0.675 for Colebrook-White, and a positive deviation of 0.84 with Blasius were observed when equated with experimental outcome.

3. Results and Discussion

3-1. Heat transfer augmentation

The use of an SDBP increased HT in a specific Re range. The level of HT enhancement varied with Re, with the ratio of j/j_0 reaching its peak before declining. This trend remained consistent for all α values. Fig. 3 demonstrated that at α of 30°, the peak j/j_0 value was obtained.

The inclined deflector operated like a nozzle, initiating higher

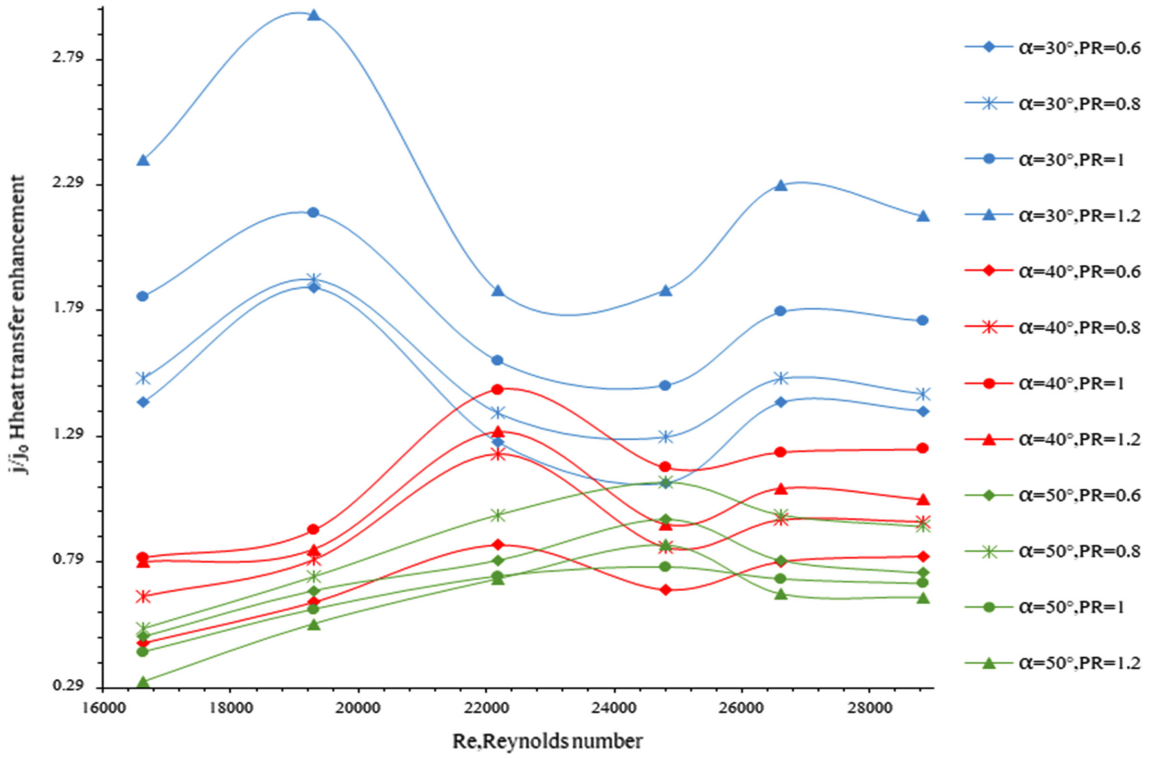

Fig. 3. Relative Colburn factor (j/j_0) vs Reynolds number.

velocities at the baffle inlet as α decreased. The baffle plate deflected the flow, increasing velocities and reducing pressure downstream. This created recirculation areas and improved fluid mixing, enhancing thermal performance. The swirling flow generated by 16 deflectors on the baffle plate swept the tube bundle, redirecting hot air to move away from the tube wall and preventing hotspots. However, a backflow eddy in baffle plate spacing could increase structural stress and pressure drop (Δp), decreasing scouring intensity upon tube wall.

As the *Re* raised, so did the velocity of the flow. This increase in speed can shorten the duration of fluid contact with the surface of the tube, where heat transfer occurred. Consequently, there may not be enough time for an efficient exchange of heat, leading to a decrease in heat transfer rates. Furthermore, when Reynolds numbers escalated, there was a possibility of the flow exhibiting a fully developed turbulent profile. This turbulent profile created a thicker resistance layer near the surface, hindering the transfer of heat. Higher *Re* might also cause stagnant and flow-recirculating zones, impeding heat flow and diminishing heat transfer efficiency. Although higher *Re* typically resembled to augmented HT rates, in this case, these led to a decay in HT as Reynolds numbers rise. Figure 3 displays the optimal *Re* range for all SDBP samples, decreasing as α surged. The HT rate in this arrangement relied on the angle of the deflector. As the angle decreased, air velocity increased, resulting in greater turbulence and intensified interaction amongst tube walls and the surrounding fluid. Therefore, high HT was amongst the tube walls and HX fluid. The α of the deflector notably amplified the HT surface area of air in contact, causing increased energy loss owing to viscosity adjacent to tube/duct walls. A rise in Δp inevitably accompanied the surge in HT rate.

The turbulence in the air flow stream could have a wide range of positive/negative effects. Turbulence augmented fluid mixing and thermal exchange, which could be beneficial in certain situations. However, undue turbulence can surge energy consumption and negative consequences like excessive noise and corrosion. The investigation by Wang *et al*. [28], as shown in Figure 4, emphasized the importance of PR. The improvement in HT was unswervingly related to the vortex flow formed downstream, whose formation was dependent on α and PR. If PR was too minor for a given α value, it might negatively affect the HT rate by escalating the interaction between vortex and core flow. Therefore, it was vital to have an appropriate PR to optimize HT while reducing Δp. Modifications in PR can led to fluctuations in HT rate as a result of heightened disturbance produced by the fluid movement between the baffles. The highest values of relative Colburn factor (j/j_0) were detected at lower α and highest PR with its values 1.03 times higher than HX without baffle plate at PR equals 1.2, and α equals 30°.

3-2. Relative friction factor

The *Re* was employed for the construction of a graph illustrating the proportionate friction factor (f/f_0) for various SDBP models, as

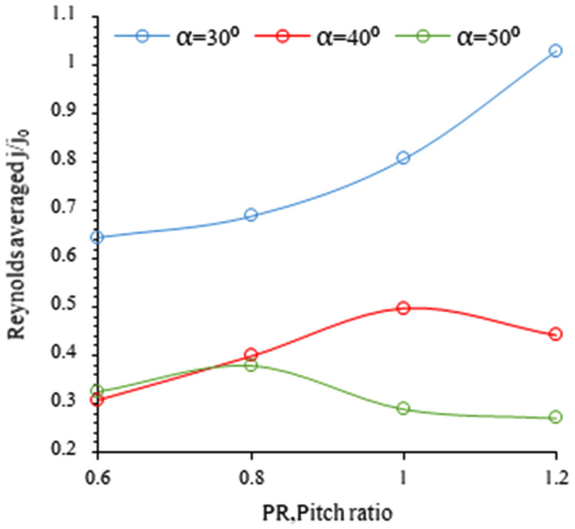

Fig. 4. Reynolds avg (j/j_0) vs Pitch ratio.

portrayed in Figure 5. The figure showcases increased f/f_0 values for SDBP due to the blockage in the fluid flow pathway. SDBP models exhibited an analogous trend, with insignificant values at lower *Re* and a subsequent escalation with higher Reynolds numbers. Equation 9 was utilized for the determination of the friction factor, which grown as Reynolds numbers increased due to the development of turbulence. Turbulent flow consumed more energy than laminar flow, resulting in higher pressure losses. Turbulence generated swirls, eddies, and vortices, enhancing fluid mixing and causing additional resistance to flow. Consequently, Δp raised.

Additionally, at α = 30°, the airflow area was at its narrowest, and the velocity was at its peak, leading to maximum flow irregularities, better mixing, more considerable energy dissipation, and hence the highest flow resistance. Consequently, the data illustrated a drop in pressure from the highest to the lowest α (α = 30°, 40°, 50°). The study demonstrated that decreasing the α to 30° ominously intensified airflow obstruction and turbulence, causing enhanced HT but at the cost of increased frictional losses due to the formation of regions with higher turbulence and larger contact area between fluid and surface, leading to substantial Δp. The highest f/f_0 values were detected at lower PR, which declined subsequently with the rise in PR. Reducing the PR reduced baffle spacing, creating fluid to recirculate between the confined space and increasing fluid and HX/tube surface contact. Also, fluid flow direction underwent significant changes once it left the narrow gap from the first baffle and reached the second baffle, where the flow reversal occurred. This increased wall shear stress, and the fluid molecules interaction increased, consequential in more significant momentum and energy exchange/changes, causing the rise in Δp. Thus, the deflector surface area enabled a more vital interaction amongst the fluid and the tube/HX/baffles wall, ultimately causing an amplified pressure drop.

Figure 6 demonstrated a downward fashion in the *Re* averaged f/f_0 as the PR and the α increased. The extreme value of 0.70 was

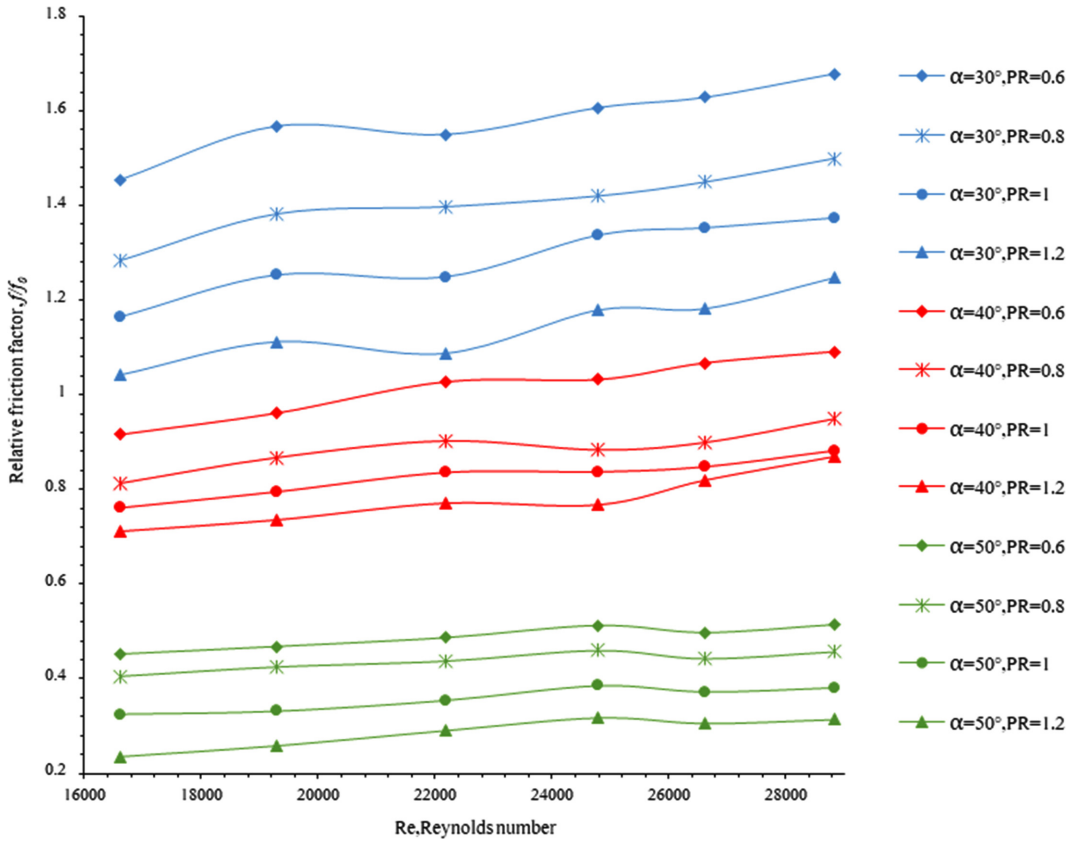

Fig. 5. Relative friction factor (f/f_0) vs Reynolds number.

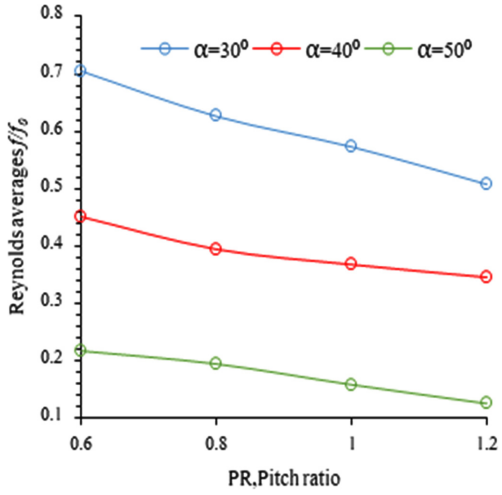

Fig. 6. Reynolds avg (f/f_o) vs Pitch ratio.

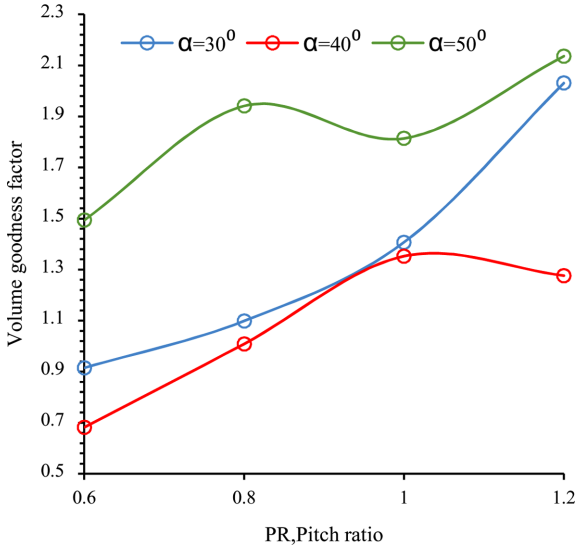

Fig. 7. Reynolds avg j/f vs Pitch ratio.

witnessed at $PR = 0.6$ when $\alpha = 30$, which was attributed to the existence of a rectangular deflector that hindered the flow of fluid, triggering a kinetic energy loss and reducing Δp. A lower α acted as an intense swirl promoter, causing a vigorous swirl flow and intensifying the vortex formation and interaction between swirl flow or secondary vortex flow and tube/duct/baffle wall; consequently, turbulence and flow recirculation increased. The vortex formation behind the deflector and flow between multiple baffles increased the flow resistance, resulting in a notable Δp rise.

3-3. Thermo-fluid performance

A novel measurement termed the TEF was used to gauge the effectiveness of the HX. This quotient was computed by dividing j by f, and the Re averaged value was displayed in Figure 7. Moreover, Figure 8 exhibits the TEF. It was evident that SDBP displayed a more noticeable augmentation in thermal amplification for shallower inclination angles, such as 30° or 40°, in contrast to steeper angles. The highest value of TEF within the specified range of Re was

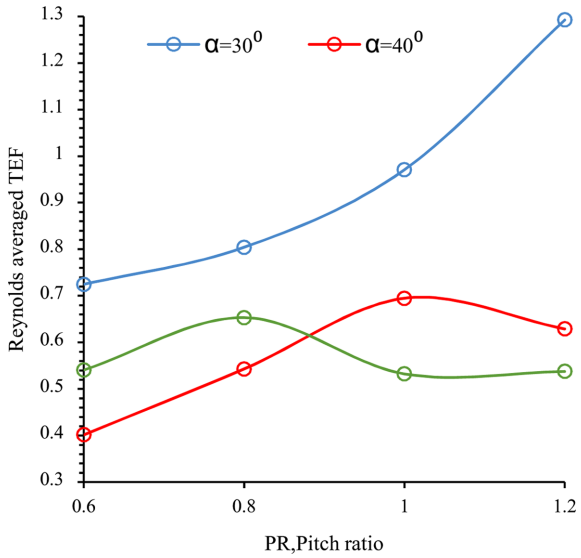

Fig. 8. Reynolds avg TEF vs Pitch ratio.

measured at 1.29 with a *PR* of 1.2 when the inclination angle (α) was set at 30°. A rise in the inclination angle led to a larger surface area exposed to the airflow, causing reduced Δ*p* and subdued TEF for SDBP.

4. Conclusions

Upon conducting a comparison of samples obtained from DBP, several notable findings were made:

(1) The velocity of flow showed a noteworthy increase when the deflector was tilted from 50° to 30°. The respective surge in velocity compared to a duct without baffles were 21.2%, 17.09%, and 9.21%.

(2) The highest value of j/j_0 was detected at smaller *Re* and smaller α values. However, optimal performance with the novel baffle design in the HX was accomplished at lower α and larger PR values.

(3) The flow resistance decreased as α values increased. On the other hand, the average relative (f/f_0) generally decreased with increasing PR, reaching its peak at *PR*=0.6.

(4) The average TEF decreased as α values increased, with the highest TEF of 1.29 observed at α=30.

(5) A duct with smaller α values experienced the greatest pressure drop, with reductions of 28.62%, 20.97%, and 16.31% for angles of 30°, 40°, and 50°, respectively, compared to a HX without baffles.

(6) The current baffle plate demonstrated effectiveness for *Re* values below 25,000, displaying superior j and *f* characteristics that degraded with *Re* rise.

(7) The impact of *Pr* was found to be insignificant, considering the operating temperature range for air as working fluid. However, further research is required to investigate the feasibility of implementing this state-of-the-art configuration in STHX, heat recovery from exhaust gas, and other industrial practices using higher-density working fluids like water, nanofluids, or mineral oil.

Acknowledgement

The authors express their gratefulness to the Mechanical Engineering Department at BIT-Mesra, India, for their support, resources, and motivation.

Nomenclature

HX : Heat exchanger
Nu : Nusselt number
TEF : Thermal enhancement factor
PR : Pith ratio
BR : Blockage ratio
D : Duct inner diameter
d : Tube outer diameter
D_h : Hydraulic diameter
Q : Heat transfer rate for air [Watts]
Δt_{lm} : LMTD
I : Distance between baffle plate [m]
A_p : Heat transfer surface area [m^2]
k_p : Thermal conductivity of Plexiglass (W/mK)
λ : Thermal conductivity of air
Pr : Prandtl number of air
X : Cross-sectional area of the duct
j : Colburn factor
STHX : Shell and tube HX
HT : Heat transfer
D_e : Equivalent diameter [m]
Re : Reynolds number
f : Friction factor
SDBP : Shutter Deflector baffle plate
μ : Coefficient of dynamic viscosity [kg/m·s]
v : Average axial velocity [m/s]
Δ*p* : Pressure drop is the test section's [Pa]
Δp_o : Pressure drop in orifice plate in [Pa]
α : Inclination angle
A_c : Flow area [m^2]
k_t : Thermal conductivity of Copper tube [W/mK]
ρ : Density of air [kg/m^3]
h_m : Avg convective heat transfer coefficient [$W/m^2 \cdot K$]
PEC : Performance enhancement factor
VG : Vortex generator
P : Area of rectangular perforation

References

1. Birch, M. J., Doig, R., Francis, J., Parker, D. and Zhang, G., "A Review of Vortex Amplifier Design in the Context of Sellafield Nuclear Operations. Proceedings of the ASME 2009 12th International Conference on Environmental Remediation and Radioactive Waste Management, Vol. 2. Liverpool, UK, 161-183. ASME (2009).

2. Abdullah A. Azhari, Ahmad H. Milyani, Nidal H. Abu-Hamdeh, and Amira M. Hussin, "Thermal Improvement of Heat Exchanger with Involve of Swirl Flow Device Utilizing Nanomaterial," *Case Studies in Thermal Engineering*, **44**, 102793(2023).
3. Wang, J., Wang, Y. and Han, J., "Experimental Investigation on Separation Characteristics of Axial Cyclone Separator," *Sci. China Technol. Sci.*, 2023.
4. Skripkin, S. G., Sharifullin, B. R. and Naumov, I., "Dual Vortex Breakdown in a Two-fluid Whirlpool," *Sci Rep*., **11**, 23085(2021).
5. Sheha, A., Ibrahim, K. A., Abdalla, H. A., El-Behery, S. M. and Sakr, I. M., "Improvement of the Axial-Jet-Pump Performance using Modified Mixing Chamber Configuration and Inlet Swirling Flow," *Scientia Iranica*, 2023.
6. Lv, P., Zhang, Y., Wang, Y. and Wang, B., "Experimental Investigation on the Influence of Swirl Ratio on Tornado-like Flow Fields by Varying Updraft Radius and Inflow Angle," *Atmosphere*., **14**(9), 1425(2023).
7. Bai, W., Liang, D., Chen, W. and Minking, K., Chyu Investigation of Ribs Disturbed Entrance Effect of Heat Transfer and Pressure Drop in Pin-fin Array," *Applied Thermal Engineering*, **162**, 114214(2019).
8. Chen, Z., Wang, H., Zhuo, J. and You, C., "Experimental and Numerical Study on Effects of Deflectors on Flow Field Distribution and Desulfurization Efficiency in Spray Towers," *Fuel Processing Technology*, **162**, 1-12(2017).
9. Khetib, Y., Alahmadi, A. A., Alzaed, A., Azimy, H., Sharifpur, M. and Cheraghian, G., "Effect of Straight, Inclined and Curved Fins on Natural Convection and Entropy Generation of a Nano fluid in a Square Cavity Influenced by a Magnetic Field," *Processes*, **9**(8), 1339(2021).
10. Lu, Z., Tao, R., Yao, Z., Liu, W. and Xiao, R., "Effects of Guide Vane Shape on the Performances of Pump-turbine: A Comparative Study in Energy Storage and Power Generation," *Renewable Energy*, **197**, 268-287(2022).
11. Liu, F. and Zhang, G., "Study on Melting and Solidification Performances Improvement of Phase Change Material Using Novel Branch Fin Structure," *Journal of Energy Storage*, **63**, 107097 (2023).
12. Hussein, M. A. and Hameed, V. M., "Experimental Investigation on the Effect of Semi-circular Perforated Baffles with Semi-circular Fins on Air–Water Double Pipe Heat Exchanger," *Arab J Sci Eng.*, **47**, 6115-6124(2022).
13. Bahuguna, R., Mer, K. K. S., Kumar, M. and Chamoli, S., Entropy Generation Analysis in a Tube Heat Exchanger Integrated with Triple Blade Vortex Generator Inserts, Energy Sources, Part A: Recovery, Utilization, and Environmental Effects, 2021.
14. Ajarostaghi, S. S. M., Karouei, S. H. H., Alinia-kolaei, M., Karimi, A. A., Zadeh, M. M. and Sedighi, K., "On the Hydrothermal Behavior of Fluid Flow and Heat Transfer in a Helical Double-Tube Heat Exchanger with Curved Swirl Generator; Impacts of Length and Position," *Energies*, **16**, 1801(2023).
15. Keat Goh, L. H., Hung, Y. M., Chen, G. M. and Tso, C. P., "Entropy Generation Analysis of Turbulent Convection in a Heat Exchanger with Self-rotating Turbulator Inserts," *International Journal of Thermal Sciences*, **160**, 106652(2021).
16. Rahman, M. A. and Dhiman, S. K., "Performance Evaluation of Turbulent Circular Heat Exchanger with a Novel Flow Deflector-type Baffle Plate," *Journal of Engineering Research*, 100105(2023).
17. Rahman, M. A. and Dhiman, S. K., "Investigations of the Turbulent Thermo-fluid Performance in a Circular Heat Exchanger with a Novel Flow Deflector-type Baffle Plate," Bulletin of the Polish Academy of Sciences Technical Sciences, 2023.
18. Rahman, M. A., "Study the Effect of Axially Perforated Baffle Plate with Multiple Opposite-oriented Trapezoidal Flow Deflector in An Air–water Tubular Heat Exchanger," *World Journal of Engineering*, 2024.
19. Rahman, M. A., "Experimental Investigations on Single-Phase Heat Transfer Enhancement in an Air-To-Water Heat Exchanger with Rectangular Perforated Flow Deflector Baffle Plate," *International Journal of Thermodynamics*, 1-9(2023).
20. Rahman, M. A., "Effectiveness of a Tubular Heat Exchanger and a Novel Perforated Rectangular Flow-deflector Type Baffle Plate with Opposing Orientation," *World Journal of Engineering*, 2023.
21. Rahman, M. A., "Thermo-Fluid Performance Comparison of an In-Line Perforated Baffle with Oppositely Oriented Rectangular-Wing Structure in Turbulent Heat Exchanger," *International Journal of Fluid Mechanics Research*, 2024.
22. Rahman, M. A., "The Effect of Triangular Shutter Type Flow Deflector Perforated Baffle Plate on the Thermofluid Performance of a Heat Exchanger," *Heat Transfer*., **53**, 939-956(2024).
23. Rahman, M. A., "The Influence of Geometrical and Operational Parameters on Thermofluid Performance of Discontinuous Colonial Self-swirl-inducing Baffle Plate in a Tubular Heat Exchanger," *Heat Transfer*, 2023.
24. ASHRAE Handbook Fundamental, American society of heating, Refrigerating and air-conditioning engineers, SI-ed., Inc., Atlanta, chap. **13**, 14-15(1993).
25. Coleman, H. W. and Steele, W. G., "Experimentation, Validation, and Uncertainty Analysis for Engineers," *John Wiley & Sons*, 2018.
26. Cao, Y. Z., "Experimental Heat Transfer, first ed. National Defence Industry Press, Beijing 1st ed., 120-125(1998).
27. Gnielinski, V., "New Equations for Heat and Mass Transfer in Turbulent Pipe and Channel Flow," *Int. Chem. Eng.*, **16**, 359-368 (1976).
28. Dittus, F. W. and Boelter, L. M. K., "University of California at Berkley," *Publication on Engineering*, **2**, 443(1930).
29. Blasius, H., Das Ähnlichkeitsgesetz bei Reibungsvorgängen in Flüssigkeiten, Forschungsheft des Vereins Deutscher Ingenieure: Berlin, Germany, 131(1913).
30. White, F. M., Fluid mechanics, McGraw-Hill, Boston (2003).

Authors

Md Atiqur Rahman: PhD, Department of Mechanical Engineering, Birla Institute of Technology, Mesra, 835215, India; rahman.md4u@gmail.com